Charge exchange x-ray emission in the near-earth environment: Simulations in preparation for the smile magnetospheric mission

Y. Tkachenko, Dimitra Koutroumpa, Ronan Modolo, H. Connor, S. Sembay

SF2A 2021
A. Siebert, K. Baillié, E. Lagadec, N. Lagarde, J. Malzac, J.-B. Marquette, M. N'Diaye, J. Richard, O. Venot (eds)

CHARGE EXCHANGE X-RAY EMISSION IN THE NEAR-EARTH ENVIRONMENT: SIMULATIONS IN PREPARATION FOR THE SMILE MAGNETOSPHERIC MISSION

Y. Tkachenko[1], D. Koutroumpa[2], R. Modolo[2], H. Connor[3] and S. Sembay[4]

Abstract. Solar Wind Charge exchange X-ray (SWCX) imaging of the Earth's magnetosheath will be the target of the Solar wind Magnetosphere Ionosphere Link Explorer (SMILE), a joined ESA-CAS mission. The mission aims to study the solar wind-magnetosphere coupling through simultaneous X-ray and UV imaging and in situ plasma and magnetic field measurements. We present simulations of the SWCX emission produced in the Earth's magnetosheath, developped in the framework of the Modeling Working Group (MWG, `https://smile.alaska.edu/`) which provides modeling support for the SMILE mission. The goal of the current study is to extend the application of a Test Particle model to input electric and magnetic fields from MHD simulations, and compare the X-ray emissivity maps to the ones from a pure MHD approach.

Keywords: Earth, exosphere, magnetosphere, Solar Wind, charge exchange, soft X-rays

1 Introduction

Generally associated with hot and energetic plasmas, soft X-ray emission was discovered in ROSAT observations of comet Hyakutake (Lisse et al. 1996) and identified as Solar Wind Charge exchange (SWCX; Cravens 1997): highly charged ions from the 1MK solar corona extract electrons from cometary neutrals and the newly created excited ions emit soft X-rays as they de-excite to their ground state. Soon, it became obvious that neutral targets would include the Earth's hydrogen geocorona, other planets' exospheres, and the interplanetary medium (Cox 1998; Cravens 2000; Dennerl 2002).

While an unpredictable nuisance for X-ray astrophysics (e.g., Snowden et al. 1995, 2004; Ezoe et al. 2011), geocoronal SWCX was recognised as a potential diagnostic goldmine for solar-terrestrial interactions (Sibeck et al. 2018). Dedicated space missions, such as SMILE (Branduardi-Raymont et al. 2020), will target this emission as an imaging tool to study the dynamic response of the Earth's magnetosphere to the solar wind (SW) impact in a global manner. The SMILE MWG has been organized to support the mission and in particular the Soft X-ray Imager science (SXI; Sembay et al. 2016). Among other, the MWG's main goals are to provide unified input parameters for magnetohydrodynamic (MHD) models of the SW-magnetosphere interaction and SWCX emission, help define the mission science requirements and potential observation geometries, and investigate magnetopause boundary reconstruction techniques from SXI images (Sun et al. 2020; Connor et al. 2021).

This proceeding focuses on a complementary approach to calculate the geocoronal SWCX emission using a Test-Particle (TP) simulation with electric (E) and magnetic (B) field input from the OpenGGCM (Open Geospace General Circulation Model; Raeder et al. 1998) MHD model. Our aim is to compare the TP X-ray emissivity maps to the ones from a pure MHD model and investigate kinetic effects that the TP approach introduces. We briefly describe the MHD and TP approaches to geocoronal SWCX calculation in section 2. In section 3, we present the simulation results: we discuss the various diagnostics performed for a single reference SW ion (O^{7+}) to estimate input parameter sensitivity in section 3.1, we present total intensity maps of the SWCX emission produced by all highly charged SW ions relevant to the SXI energy range, and subsequent synthetic SXI images in section 3.2. Finally, we offer some conclusions and perspectives in section 4.

[1] Université d'Orléans, Orléans, France
[2] LATMOS, CNRS, UVSQ Paris-Saclay, Sorbonne Université, Guyancourt, France
[3] University of Alaska Fairbanks, Fairbanks AK, USA
[4] University of Leicester, Leicester, UK

2 Model Description

The TP model describes the dynamic of charged particles in a static electromagnetic field environment. It solves the equation of motion with a basic leap-frog pusher and a predictor-corrector scheme to determine the acceleration of the particles. The E and B field description comes from the OpenGGCM MHD model simulation with SW input of $n_p = 12.5\ cm^{-3}$, $v_p = 400\ km/s$, and $T = 20,000\ K$, the IMF input of $(B_x, B_y, B_z) = (0, 0 - 5)\ nT$, and no dipole tilt. For the TP simulation, we used a uniform cartesian grid covering the spatial domain $0 \leq X_{GSE} \leq 20R_E$, $-10R_E \leq Y_{GSE}, Z_{GSE} \leq +10R_E$ with an adaptable spatial resolution $ds = 0.05$ or $0.1\ R_E$. For each simulation, 37.5M test-particles representing a given ion species X^{q+} are launched from the entry face of the simulation ($X_{GSE} = 20R_E$) with plasma properties corresponding to the SW characteristics of the OpenGGCM MHD simulation.

During the motion of the particle, at each time step, we compute the SWCX production associated with the reaction

$$X^{q+} + H \longrightarrow X^{(q-1)+} + H^{+} \tag{2.1}$$

with X^{q+} the parent solar wind ions, H geocoronal targets, $X^{(q-1)+}$ the produced ions and H^+ the newly born planetary protons. The number of produced ions is determined by the number of parent ions lost at a particular position in space and as a function of time, according to the equation:

$$\frac{\partial N_{X^{q+}}}{\partial t} = -N_{X^{q+}} \times \sigma_{X^{q+},H} \times v_{X^{q+}} \times n_H \tag{2.2}$$

with $N_{X^{q+}}$ the number of physical ions, $\sigma_{X^{q+},H}$ the CX cross-section between parent ions and H atoms, $v_{X^{q+}}$ the speed of the parent ions (the neutral atoms' speed is negligible), and n_H the geocoronal neutral density. The n_H density distribution is given by Cravens et al. (2001). To obtain the total SWCX production rate for an ion species (proportional to the SWCX emissivity), we sum the production rate contributed by each test-particle in the cartesian grid. The emissivity $Q_{TP}^{X^{q+}}$, is then calculated by multiplying by the relative abundance of the ion species, and their characteristic soft X-ray emission line probabilities (in eV). Simulations have been performed for 21 parent ion species ($C^{5,6+}$, $O^{7,8+}$, $N^{6,7+}$, $Ne^{8,9+}$, $Mg^{8,9,10,11+}$, $Si^{8,9,10+}$, $S^{8,9+}$, $Fe^{8,9,10,11+}$), producing main SWCX emission lines in the SXI energy range (0.2 - 2.0 keV). The total TP emissivity Q_{TP} in the SXI bandpass is then calculated as the sum of individual $Q_{TP}^{X^{q+}}$ emissivities.

In the pure MHD approach, the total emissivity Q_{MHD} is calculated as in Cravens et al. (2001): $Q_{MHD} = \alpha \times n_p \times v_p \times n_H$, where $n_p \times v_p$ is the MHD SW proton flux, and α combines all cross-section, ion abundance and line emission probability information for the list of ions above.

3 Results

3.1 O^{7+} SWCX Emissivity

We performed several TP simulations for reference ion O^{7+} to estimate the sensitivity of the results to input parameters. First we test velocity-dependent CX cross-sections, and conclude that they do not have a significant impact in the specific SW velocity regime considered here. Fig.1 shows a side view of the TP results on the O^{7+} SWCX emissivity for different spatial and time-step resolutions (panels b, c, d, e & f), in comparison with MHD results for the same ion (panel a). The single-fluid MHD shows a continuous emissivity gradient, while the TP simulations exhibit small scale structures due to kinetic effects, such as streamlines that ions follow due to the superposition of the gyromotion and the bulk flow, as well as regions of re-acceleration of the ion plasma flow just above and below the subsolar region. A finer spatial resolution (panel c) also highlights a ripple effect due to magnetic overshoot at the bow shock crossing (marked by a white arrow in the zoomed-in panels of the subsolar bow-shock; Masters et al. 2013). Nevertheless, once all the TP results of individual ions (with different gyroradii) are combined in the projected SWCX intensity maps (see section 3.2 and Fig.2), this effect does not seem quite as conspicuous. On the other hand, a higher temporal resolution seems decisive. As the time step becomes smaller, the description of the charged particles penetration into the cusps improves (compare panels d, e & f) and simulations show that charged particles stay in the cusps longer producing higher X-ray emission.

3.2 Total Intensity maps and SXI Synthetic Images

The total SWCX intensity maps (from all 21 ions) were then calculated with the MHD and TP approaches in various observation geometries (Fig.2). Columns (a) and (b) present emission maps integrated along the main

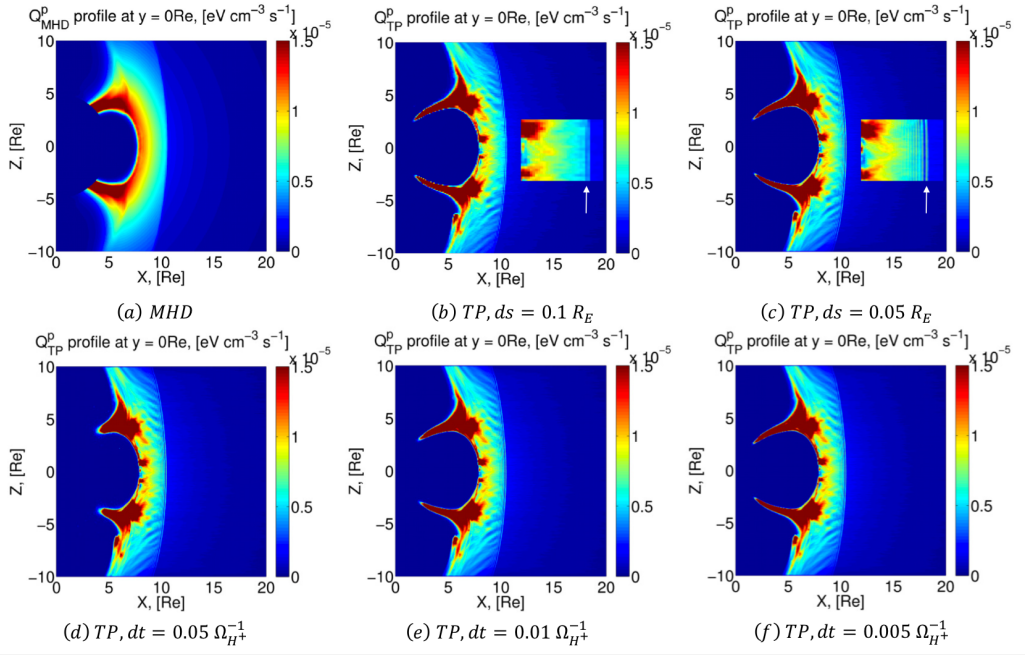

Fig. 1. MHD-calculated (a) and TP-calculated (b, c, d, e & f) production rate (emissivity) cuts along the noon meridian (XZ plane, at Y = 0 R_E) for emission lines produced by SWCX of the reference ion O^{7+}. For the TP-calculated cuts, (b) & (c) compare simulation results for two different spatial resolutions (zoomed-in panels of the subsolar bow-shock highlight the magnetic overshoot), and (d), (e) & (f) compare simulation results for different time step resolutions.

simulation axes. The location of the magnetopause in the two models is consistent and its distance to the Earth along the X-axis is about 7 - 7.5 R_E, where the MHD maximum emission drops in both XY and XZ planes (top a-, b-panels). In the TP case, moving from +X to -X, the emission starts rising around the same region as the MHD, but in the XY plane (bottom a-panel) the cusps intense emission (integrated along Z) widens the emission region even inward from the magnetopause (< 7 R_E). In the XZ plane (Fig.2 - b), the TP emission starts and drops around the same regions as the MHD, except that the kinetic effects give more structure and higher intensity along the magnetopause in the re-acceleration regions close to the X-axis. Also the pre-cusp regions are much brighter in the TP results.

The produced MHD and TP total ion data cubes were then used as input to the SXI instrument simulation software to produce a realistic SXI observation from orbit (Fig. 2 - c, d). The SMILE spacecraft was positioned at $\vec{r}$ = (3.76, 7.46, 17.97) R_E, the SXI field of view was aimed at $\vec{p}$ = (8.04, 0.00, 0.00) R_E and the Earth limb angle was 20.48°. Column (c) plots show the projected simulation maps and column (d) plots show the synthetic detector images for a typical exposure time of 300 s with simulated noise sources included. Despite the synthetic observations' noise, it is obvious that the TP simulations yield higher intensity over a wider region.

4 Conclusions and Perspectives

We have performed TP simulations of the SWCX emission in the Earth's geocorona, compared the results to equivalent MHD simulations, and produced realistic synthetic images through the SMILE/SXI instrument simulator. The TP simulations are consistent with the existing MHD model. At the same time, TP results exhibit more complex structure, highlighting kinetic effects such as re-acceleration regions, while also generating more intense soft X-ray emissivity in general.

We have also tested the sensitivity of TP results to several parameters (dynamic cross-sections, spatial and temporal resolution), of which the temporal resolution was the most crucial for the proper description of ion trajectories in the cusps. An advance on this parameter would be to use an adaptive time step through the simulation grid. This would potentially help optimize the required numerical ressources.

Future work includes TP simulations for different E & B configurations and SW conditions, like ICMEs (Interplanetary Coronal Mass Ejections). Such events may push the magnetosheath boundaries inward where

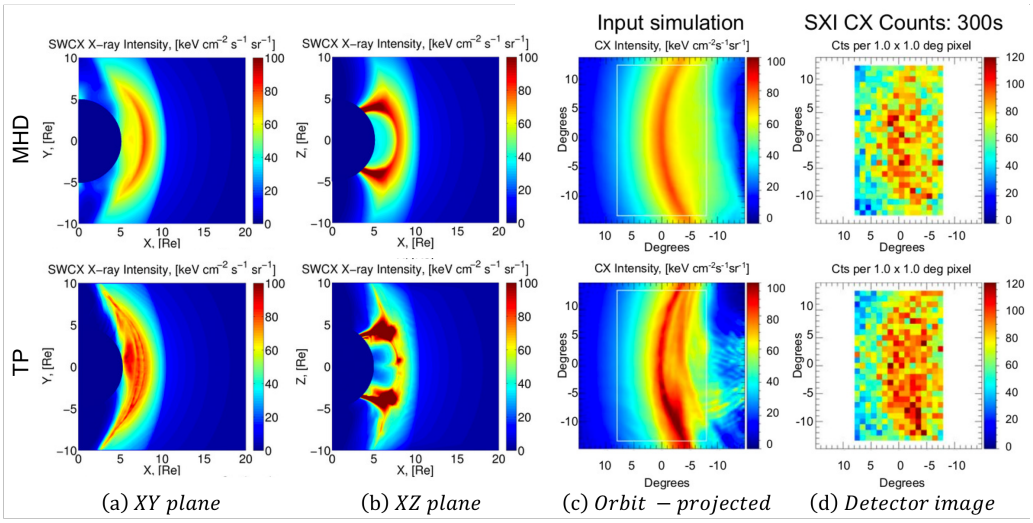

Fig. 2. X-ray intensity maps for MHD (top) and TP (bottom) simulations integrated along the simulation box main axes Z (a) and Y (b), and from a simulated SMILE orbit (c - the white rectangle represents the SXI field-of-view). Column (d) shows the corresponding synthetic SXI images for a typical 300 s exposure. See text for details.

neutral H density is larger while high energy SW particles may penetrate through the magnetopause as well as deeper into the cusps. In addition, changes in SW ion thermal velocities and SW elemental composition (and thus relative SWCX spectral line strength) may require the use of TP simulations where the consideration of each ion separately may prove to be an advantage over MHD models.

Finally, we will produce synthetic SXI observations for different geometry configurations (including the highly emissive cusp regions), to be tested with the boundary tracing methods developed by the SMILE MWG.

This work is supported by CNES. To process the SWCX test-particle simulations data, this study benefited from the IPSL mesocenter ESPRI facility which is supported by CNRS, UPMC, Labex L-IPSL, CNES and Ecole Polytechnique. H. K. Connor gratefully acknowledges support from the NASA grants 80NSSC18K1043, 80NSSC20K1670, and 80MSFC20C0019. The SXI simulation software is supported by UKSA.

References

Branduardi-Raymont, G., Wang, C., Escoubet, C. P., et al. 2020, in EGU General Assembly Conference Abstracts, EGU General Assembly Conference Abstracts, 10783

Connor, H. K., Sibeck, D. G., Collier, M. R., et al. 2021, Journal of Geophysical Research (Space Physics), 126, e28816

Cox, D. P. 1998, Modeling the Local Bubble, ed. D. Breitschwerdt, M. J. Freyberg, & J. Truemper, Vol. 506, 121–131

Cravens, T. E. 1997, Geophys. Res. Lett., 24, 105

Cravens, T. E. 2000, Advances in Space Research, 26, 1443

Cravens, T. E., Robertson, I. P., & Snowden, S. L. 2001, Journal of Geophysical Research: Space Physics, 106, 24883

Dennerl, K. 2002, A&A, 394, 1119

Ezoe, Y., Miyoshi, Y., Yoshitake, H., et al. 2011, PASJ, 63, S691

Lisse, C. M., Dennerl, K., Englhauser, J., et al. 1996, Science, 274, 205

Masters, A., Slavin, J. A., Dibraccio, G. A., et al. 2013, Journal of Geophysical Research (Space Physics), 118, 4381

Raeder, J., Berchem, J., & Ashour-Abdalla, M. 1998, J. Geophys. Res., 103, 14787

Sembay, S., Branduardi-Raymont, G., Drumm, P., et al. 2016, in AGU Fall Meeting Abstracts, SM44A–04

Sibeck, D. G., Allen, R., Aryan, H., et al. 2018, Space Sci. Rev., 214, 79

Snowden, S. L., Collier, M. R., & Kuntz, K. D. 2004, ApJ, 610, 1182

Snowden, S. L., Freyberg, M. J., Plucinsky, P. P., et al. 1995, ApJ, 454, 643

Sun, T., Wang, C., Connor, H. K., Jorgensen, A. M., & Sembay, S. 2020, Journal of Geophysical Research (Space Physics), 125, e28169